Biocatalysis and Agricultural Biotechnology 22 (2019) 101436

Contents lists available at ScienceDirect

Biocatalysis and Agricultural Biotechnology

journal homepage: http://www.elsevier.com/locate/bab

Facile biofabrication, characterization, evaluation of photocatalytic, antipathogenic activity and *in vitro* cytotoxicity of zinc oxide nanoparticles

Krishnasamy Sekar Rajkumar [a], Sridhar Arun [a], Manikandan Dinesh Babu [a], Perumalsamy Balaji [b], Srinivasan Sivasubramanian [c], Venkatasamy Vignesh [d], Ramasamy Thirumurugan [a, b, *]

[a] *Laboratory of Aquabiotics/Nanoscience, Department of Animal Science, School of Life Sciences, Bharathidasan University, Tiruchirappalli, 620 024, Tamil Nadu, India*

[b] *UGC-National Center for Alternatives to Animal Experiments, Bharathidasan University, Tiruchirappalli, 620 024, Tamil Nadu, India*

[c] *King Institute of Preventive Medicine & Research, Chennai, 600 032, Tamil Nadu, India*

[d] *Animal Quarantine and Certification Service, Department of Animal Husbandry, Dairying and Fisheries, Ministry of Agriculture & Farmers Welfare, Mumbai, India*

ARTICLE INFO

Keywords:
Allium cepa
Foodborne illness
Antipathogenicity
Phytochemistry
Nuclear fragmentation
Apoptosis

ABSTRACT

Zinc oxide nanoparticles (ZnO NPs) are gaining interest due to their multifunctional properties and desirable biological activities. The present study reports the formulation and characterization of ZnO NPs using an aqueous extract of dry onion peels (*Allium cepa* L) and further investigates their photocatalytic, *in vitro* antipathogenic activity and cytotoxicity against human lung cancer A549 cell line. The results of XRD analysis showed the presence of nine intense peaks indicating the crystallized hexagonal phase of ZnO NPs with a size of about 35 nm. Field-emission scanning electron micrographs and the results of EDS showed the hexagonal morphological feature, and the presence of zinc and oxygen in phytogenically synthesized ZnO NPs. The synthesized ZnO NPs showed potent catalytic activity in the degradation of organic dyes (crystal violet and methylene blue). The formulated ZnO NPs indicated a significant bactericidal activity against *Bacillus* sp., *Escherichia coli, Staphylococcus aureus, Vibrio cholerea, Corynebacterium* sp., and *Salmonella* sp. that are common foodborne pathogens. In this study, the obtained IC_{50} concentration of 51.25 μg/mL exhibits significant anticancer activity against A549 cells than other tested concentrations because of the release of zinc ions, which induce the cell apoptosis. Furthermore, studies on cell cycle validate that ZnO NPs arrest the cell cycle at the sub-G_1 phase of A549 cells. These results suggest the utility of phytogenic ZnO NPs for various biomedical applications.

1. Introduction

Nanoparticles have immense potentials due to their diverse biological functional spectrum, therapeutic efficacy, and safety (Ovais et al., 2018). In recent times, much of the research studies focus on developing novel multifunctional nanoparticles (NPs) with improved functions and a range of metals such as gold, silver, copper, aluminum, metal oxides like zinc, titanium and magnesium oxides have been explored for wide-ranging features including antibacterial and anticancer properties (Cai et al., 2018; Hoseinnejad et al., 2018). In the medical field, NPs are used as a coating material for preventing the microbial bloom and act as an anti-bio-film agent (Pugazhendhi et al., 2018c). Nanoparticles prepared from Zn, Fe, and Cu metal oxides have merits over the noble metals such as silver and gold owing to their techno-economic viability by means of formulation and utility (Yang et al., 2018). Among these metal oxides, ZnO NPs have received much attention in recent times, and are considered as one of the most promising materials because of their high catalytic and optical property, bio-conductivity, antimicrobial and anticancer activity (Darroudi et al., 2014; Malakootian et al., 2019). Zinc is an essential microelement for cell division, growth, and breakdown of enzymes and proteins in humans. It is needed for the immune system and protects the skin from aging, sun, and wind (Prasad, 2014). ZnO is contemplated as "generally recognized as safe" (GRAS) by food and drug

* Corresponding author. Department of Animal Science, School of Life Sciences, Bharathidasan University, Tiruchirappalli, 620 024, Tamil Nadu, India.
E-mail address: ramthiru72@bdu.ac.in (R. Thirumurugan).

https://doi.org/10.1016/j.bcab.2019.101436
Received 25 August 2019; Received in revised form 6 November 2019; Accepted 16 November 2019
Available online 17 November 2019

Administration (FDA) of the USA (Rasmussen et al., 2010). In addition, to this ZnO NPs are used as an ingredient in plastics, glass, ceramics, rubber, battery, a dietary source in the food, antifungal, and antibiofilm agents (Ma et al., 2013; Pugazhendhi et al., 2018b). Interestingly, physico-chemical attributes such as wide band-gap (3.3 eV), high exciton binding energy (60 eV), high temperature, and UV stability and non-toxicity enable researchers to opt ZnO NPs over other metal oxides. Several strategies have reported the synthesis of NPs including physical and chemical methods. However, this methods suffer limitations such as the requirement of high performance equipment, processes involving high temperature, pressure and thermal evaporation and more importantly, the generation of toxic by-products or use of toxic chemicals for preparation of NPs posing threat to environment, health and safety (Rajkumar et al., 2016; Shah et al., 2018; Sukhanova et al., 2018).

These limitations associated with conventional physico-chemical methods necessitate researchers to develop nano-approaches using greener routes including the synthesis of NPs by phytogenic method, which has high efficiency in performance, show non toxicity, and possess economic and environmental viability (Khan et al., 2019; Mayedwa et al., 2018; Seabra, 2018). Besides, phytogenic synthesis of NPs possesses not only biomedical potential but also the desired characteristics such as varying structure and functional features especially phytochemical associated therapeutic nature and circulation stability, and high processivity with preferable ADME pharmacological features (Iqbal et al., 2019; Khalil et al., 2018; Rahman et al., 2019). The merits of phytogenic NPs are not only attributed to the metal components in NP synthesis but also to the plant metabolites such as alkaloids, phenolic acids, proteins, terpenoids, and polyphenols, which facilitate the reduction of metal ions and support the size and stability of NPs (Dzul-Erosa et al., 2018; Fakhari et al., 2019; Nasrollahzadeh et al., 2019).

Crystal violet (CV) and Methylene blue (MB) are synthetic organic dyes that are extensively used in textile, paper, and rubber industries as colouring ingredients, and they are cationic and anionic (Saha et al., 2017). These dyes are being discharged from industries without any treatment, and it can cause adverse effects on the health of the aquatic ecosystem. Therefore, we need to develop an eco-friendly method that can effectively degrade the dye effluents. Metal oxide nanoparticles are known to exhibit better catalytic activity due to their large surface to volume ratios and light-absorbing properties (Gnanasekaran et al., 2017; Rodrigues et al., 2019). Metal oxides potentially catalyze the organic dye pollutants in solar and UV lights (Pugazhendhi et al., 2019). The nanocatalyst which is recovered from the dye solution, can be reused a number of times efficiently (Saratale et al., 2018).

Cancer is one of the major causes of death (Siegel et al., 2014) in both male and female worldwide, and the incidence and mortality of lung, cervix, stomach, prostate, and breast cancer are higher among the population. Therapeutic synthetic drugs cause side effects by damaging the healthy tissues during treatment. Besides, conventional chemotherapeutics have limitations including bioavailability, drug resistance, toxicity, tumor-targeted delivery, and solubility (Pugazhendhi et al., 2018a; Sun et al., 2014; Wang et al., 2014). Metal oxide NPs have been employed to minimize several limitations, and metal oxide NPs synthesized through the phytogenic greener approach could be the best alternative drug due to the enhancement of anticancer function through bioactive constituents.

Allium cepa, an industrially important horticulture crop cultivated throughout the world, has a range of nutritional and medicinal properties including its use in Ayurveda, an ancestral discipline of medicine in India (Mhaskar et al., 2000). The onions are known for their healing potential against dyspnea, angina pectoris, cough, dysentery, and bronchial conditions. It is reported that the use of onion in human life can reduce the risk of stomach carcinoma, antimicrobial, antifungal, hypoglycemia, antihypertensive and antispasmodic effects (Ali et al., 2000; Elnima et al., 1983; Sakakibara et al., 2008; Yamamoto et al., 2005; Yin and Tsao, 1999). The dry outer layer of the onion is rich in calcium, dietary fiber, fructooligosaccharides, flavonoids, and alk(en)yl cystein sulphoxides and quercetin with antioxidant properties (Prakash et al., 2007). Though reports are available on the synthesis of NPs that contain onion phytoconstituents, the synthesis of ZnO NPs using onion peels has not been reported (Khalilzadeh and Borzoo, 2016; Sahni et al., 2015; Stan et al., 2015). In this report, the ZnO NPs were synthesized using onion peel (Brown skin) extract as a reducing and capping agent because the onion peel extract possesses antioxidant capacity and detoxification effect (Kim et al., 2013).

Hence, in this present study, ZnO NPs are synthesized by adopting a phytogenic approach using onion peels, which is discarded as waste material. Synthesized ZnO NPs were further evaluated on the photocatalytic and antipathogenic activity of synthesized NPs against foodborne illness-causing bacterial pathogens and cytotoxicity on human lung cancer A549 cell line.

2. Materials and methods

Zinc nitrate hexahydrate, yellow tetrazole, 3-(4,5-dimethylthiazol-2-yl)-2,5-diphenyltetrazolium bromide (MTT), dimethyl sulfoxide (DMSO), dulbecco's modifeid eagle medium (DMEM), fetal bovine serum (FBS), antibiotic solutions (penicillin and streptomycin), Hoechst 33258 and acridine orange were procured from HIMEDIA, Mumbai, India. Chemicals and solvents used for the preparation of plant extract were of analytical reagent grade. Human lung cancer A549 cell line was obtained from National Centre for Cell Science (NCCS), Pune, India.

2.1. Preparation of plant extract

Five g of dry brown outer onion peel were washed with running tap water followed by rinsing with distilled water and soaked in a 250 mL Erlenmeyer flask containing 50 mL of double-distilled water. The solution was boiled at 70 °C for 15 min. The peel broth was filtered through Whatman No 1 (0.25 μM) filter paper, and the filtrate was stored for further experimental purposes.

2.2. Synthesis of ZnO NPs

ZnO NPs were synthesized by dissolving 0.1 M of zinc nitrate hexahydrate (HIMEDIA, Mol. Wt. : 297.49) slowly in 20 mL of double distilled water in an Erlenmeyer flask kept under vigorous stirring at 60 °C for 60 min. About 5 mL of the plant extract was added to the aqueous solution, and the solution was made up to 100 mL. The pH of the aqueous solution was maintained at 12.0 by adding 2.0 M NaOH dropwise until the solution became pale white color and stirred continuously for 3 h by the same condition. The resultant pale white precipitate was washed with distilled water several times, followed by ethanol washing and centrifuged at 8000 rpm for 15 min. The precipitate was dried in a hot air oven. The dried pale white precipitate powder of ZnO NPs was carefully collected and used for further studies.

2.3. Characterization

The crystalline structure and size of the dried ZnO NPs were determined and confirmed by XRD analysis. The patterns of XRD was recorded using a PANalytical X'Pert Pro Powder X'Celerator Diffractometer, Netherlands. The experiments were performed at the wavelength of 1.5406 Å and operated at a voltage of 40 kV and 40 mA. It was done in the region of 2θ from 20 to 80°. Fourier transform infrared (FT-IR) spectroscopy analysis was performed to analyse the

functional groups of the synthesized ZnO NPs. The dried NPs were mixed with potassium bromide (KBr), and the FT-IR spectra were recorded in PerkinElmer Spectrum 2 in the wavenumber frequency ranged from 4000 to 500 cm^{-1}.

The microstructure and size of the ZnO NPs were assessed by field-emission scanning electron microscope (FESEM), Carl Zeiss, UK. The elemental compositions of ZnO NPs were analyzed by energy-dispersive x-ray spectroscopy. The optical properties of ZnO NPs were characterized by Synergy HT Multimode Reader (BioTek Instrument, Winooski, VT, USA), with absorption spectra of the wavelength range of 300–700 nm.

2.4. Photocatalytic dye degradation

Photocatalytic activity was investigated by the degradation of CV and MB solution at various concentrations of ZnO NPs (0.5–10 mg). A 10 mg/L stock solution of CV and MB was prepared, suitable concentrations of ZnO NPs were added to 100 mL of both CV and MB solution under constant stirring at the dark condition of equilibrium of working solution for 30 min before sunlight and UV (Philips TUV 30 W-UV light) irradiation. A control setup was also maintained without NPs. The dispersion was exposed to both light irradiation, and the suspension mixtures were withdrawn at selected time intervals (0 to 240 min for sunlight and 0 to 300 min for UV light). The rate of dye degradation was determined by using absorbance spectrum of solution and was measured in UV–visible spectrophotometer of Synergy HT Multimode Reader. Following formula was used to calculate the % of photocatalytic dye degradation

$$(\%) = \frac{C0 - Ct}{Ct} \times 100$$

Here, C_0 is the initial concentration of the dye solution, and C_t is the final concentration of the dye solution after exposure in both light sources.

2.5. Antipathogenic activity of ZnO NPs

The antipathogenic activity of synthesized ZnO NPs was evaluated using agar well diffusion method against foodborne pathogens such as *Bacillus* sp., *Escherichia coli, Staphylococcus aureus, Vibrio cholerae, Corynebacterium* sp. and *Salmonella* sp. (clinical isolates). Fresh culture of each strain was swabbed uniformly over the agar surface, and approximately 6 mm diameter wells were made by gel puncture. The different concentration of ZnO NPs (25, 50, 75, and 100 μg/μL) solution was added to the wells. Commercial antibiotic (Streptomycin, 10 μg/μL) was used as a positive control. The zone of inhibition diameter was measured after overnight incubation at 37 °C.

2.6. Cytotoxicity assay

In vitro cytotoxic activity was assessed by MTT assay (Mosmann, 1983), which determines the proportion of active human lung cancer A549 cells treated with ZnO NPs, and NPs untreated cells were used as control. Prior to the cell viability assay, the ZnO NPs were dispersed in DMSO at the concentration of 0–200 μg/mL and dispensed into the 96 well plate containing 5×10^3 density of A549 cell line. After 24 h incubation, 20 μL of MTT was added to each well and incubated for 4 h followed by the addition of 100 μL of DMSO to solubilize the MTT formazan crystals. The measurement of each well optical density was carried out on Bio-Rad iMark reader at a wavelength of 570 nm. The percentage of inhibition was calculated using the following formula:

$$= \frac{mean\ OD\ of\ control\ (Untreated\ cells) - mean\ OD\ of\ treated\ cells}{mean\ OD\ of\ control\ (Untreated\ cells)} \times 100$$

2.7. AO/EB double staining study

Apoptotic morphology of A549 cells treated by ZnO NPs was determined by acridine orange (AO) and ethidium bromide (EB) dual staining method as described by Spector et al. (1998). A549 cells were grown in 96-well plate (5×10^5 cells/well) for 24 h followed by incubation of cells at IC_{50} dose of ZnO NPs for 24 h. Then the media was discarded, and the cells were trypsinized and washed with PBS. After washing, the cells were stained with 25 μL of AO/EB, placed on a microscopic glass slide and viewed under a fluorescent microscope (Carl Zeiss, Axioscope2plus) with excitation and emission wavelengths of 450 nm and 490 nm respectively. The live cells, apoptotic cells, and necrotic cells in control and treated group were investigated.

2.8. Assessment of nuclear morphology

Cytopathology was studied by staining the nuclear chromatin of A549 cells (5×10^5) with 1 μL of Hoechst 33258 (1 mg/mL) for 5 min at 37 °C (Kasibhatla, 2006). After 5 min incubation, a drop of cell suspension was placed on a glass slide and observed in a fluorescent microscope (Carl Zeiss, Axioscope2plus) fitted with a 377–355 nm filter. The number of cells reflecting pathological changes was counted.

2.9. Measurement of mitochondrial membrane potential (MMP)

The mitochondrial membrane potential of apoptotic cells was investigated by Rhodamine 123 staining, according to the method described by Baracca et al. (2003). After the exposure of ZnO NPs at obtained inhibitory concentration, the cells were harvested and washed with PBS, which were resuspended in PBS at the concentration of 5×10^5 cells/mL and mixed with 25 μL of Rhodamine 123 dye (1 mg/mL). The mitochondrial depolarization pattern ($\Delta\psi m$) of A549 cells was observed under the fluorescent microscope.

2.10. Cell cycle arrest

Cell cycle arrest of ZnO NPs treated cells was investigated using flow cytometry to measure the % of various phases of the cell cycle using propidium iodide (PI) DNA staining. Briefly, A549 cells were seeded (5×10^5) in a six well plate and allowed to attach. Subsequently, the cells were administered the IC_{50} concentration of ZnO NPs for 24 h, washed with PBS, fixed with 70% ice-cold ethanol for 4 h, and stored at 4 °C. Ethanol fixed cell suspension was centrifuged at 1000 rpm for 5 min and washed with PBS, the suspension was again centrifuged, and the pellets were collected for flow cytometry analysis. Cell pellets were re-suspended in 750 μL of PBS, and 5 μL of RNase A was added and incubated at 37 °C for 30 min. After the incubation, the cells were stained with 75 μL of PI (1 mg/mL). The PI stained cells were incubated at room temperature for 15 min, and cell cycle profiles were obtained using FACSCalibur (Becton Dickinson, USA).

2.11. Statistical analyses

All results data were expressed as mean ± standard deviation (SD) and analyzed using SPSS 16.0 software (SPSS, Chicago, IL, USA). Triplicate experiments were carried out, and the statistical evaluations were performed by one-way analysis of variance (ANOVA). Significant differences between experimental groups and control were determined at $p < 0.05$.

3. Results and discussion

3.1. X-ray diffraction

Fig. 1a. Illustrates the XRD pattern of the bio-fabricated ZnO NPs obtained from zinc nitrate and aqueous extract of onion peel. The obtained XRD peaks were identified as (1 0 0), (0 0 2), (1 0 1), (1 0 2), (1 1 0), (1 0 3), (2 0 0), (1 1 2) and (2 0 1) corresponding to the scattering angles (2θ) of 31.87, 34.52, 36.35, 47.62, 56.68, 62.93, 66.45, 68.03 and 69.18 respectively. The obtained lattice planes are in good agreement with the previous report of ZnO NPs synthesized by Al Abdullah et al. (2017). All of these lattice planes offer a face-centered cubic (fcc) hexagonal wurtzite structure of the bio-synthesized nanoparticles (Hassan et al., 2015; Jamdagni et al., 2016). The pattern of obtained peaks is in agreement with the hexagonal phase (JCPDS File No. 79–0205). By employing the followed Debye–Scherrer equation, the average particle size of bio-synthesized nanoparticles was calculated:

$$D = K\lambda/(\beta \cos \theta)$$

where: D – particle size in nm, λ – wavelength of the X-ray radiation, β – the line width at half-maximum height (FWHM), θ Bragg's angle of diffraction (Cullity and Stock, 2001). The average size of synthesized ZnO NPs was found to be ~35 nm. Table 1 represents the particle size, and the FWHM value for each peak was used for particle size calculation. Previous studies confirm the biologically synthesized ZnO NPs size ranging from 40 – 74 nm, and the use of plant extract restricts the growth of NPs (Miri et al., 2019; Stan et al., 2015). In addition, to this some impurities are present in the XRD analysis, which peaks may be from unreacted molecules of Zn nitrate and phytochemical constituents of onion peels.

3.2. FT-IR spectra

The functional groups of synthesized ZnO NPs were analyzed by FT-IR. In Fig. 1b, the IR result shows the spectrum at 3383 cm^{-1} indicating the presence of alcohols and phenols (O–H stretch) (Miri et al., 2019). The peak in the region of 2959 cm^{-1} is attributed to alkanes (C–H stretch) (Dobrucka and Długaszewska, 2016). The bands at 1606, 1405, 1241 and 1113 cm^{-1} are corresponding to primary amines (N–H stretch) of H_2O molecules adsorbed on ZnO particles, aromatics (C–C stretch) and aliphatic amines (C–N stretch) respectively (Ambika and Sundrarajan, 2015; Šarić et al., 2017). The spectra band at 920 cm^{-1} indicates the presence of carboxylic acid (O–H stretch). The spectra recorded at the regions of 771 and 650 cm^{-1} were attributed to alkyl halides (C–CI and C–Br stretch). The characteristic peak at 602 cm^{-1} is assigned due to Zn–O with water and organic molecules (Šarić et al., 2019). These results show the presence of secondary plant metabolites functionalized on the surface of ZnO NPs and suggesting surface capping by the biomolecules (Zheng et al., 2019). In addition, owing to the presence of hydroxyl and carboxyl groups in the peel extract, facilitated the formation of ZnO NPs. This process is started when the nitrate decomposed to nitrogen dioxide and oxygen during the vigorous stirring at 60 °C, which removes the nitrogen dioxide from the compounds (Khorsand Zak et al., 2013; Yan et al., 2015). Thus, from the FT-IR spectrum, it proves the synthesized NPs contains phenols, alcohols, primary amines, and carboxylic acid. These bioactive compounds were responsible for the reduction for the stabilization of NPs (Dobrucka and Długaszewska, 2016; Senthilkumar and Sivakumar, 2014).

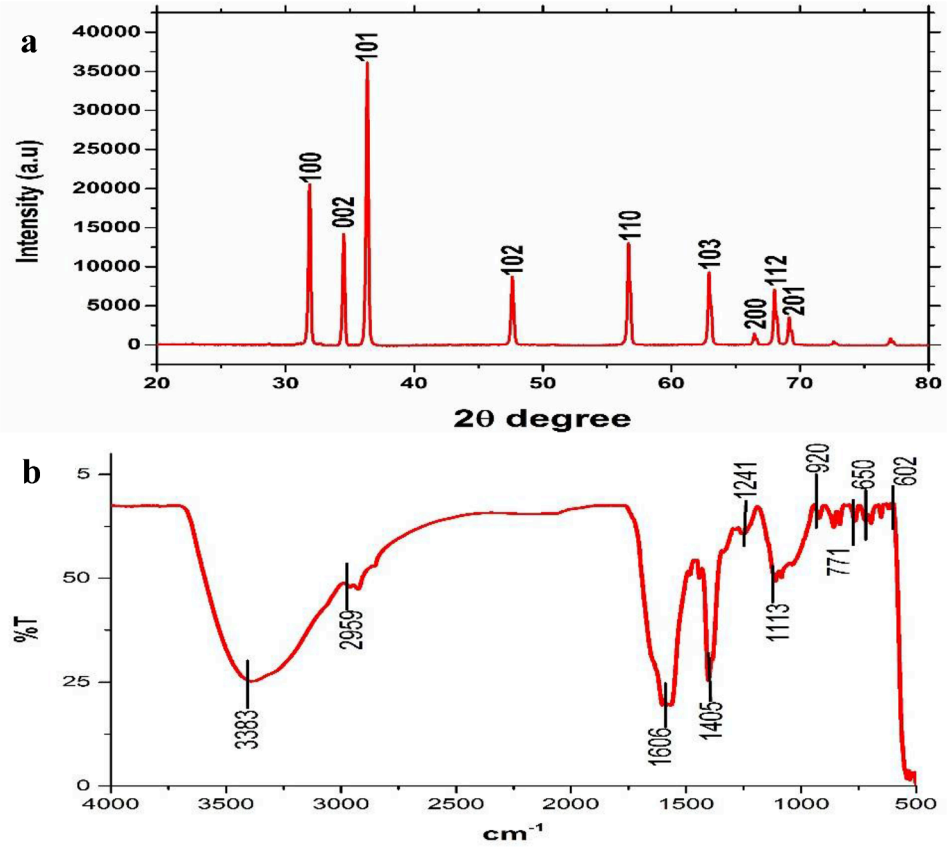

Fig. 1. (a) XRD pattern of ZnO NPs. (**b**) FTIR analysis of ZnO NPs synthesized using *Allium cepa* peel extract.

Table 1
Calculated average particles size of the synthesized ZnO Nanoparticles.

2θ Values	FWHM (β)	h k l	D (nm)
31.87	0.21336	1 0 0	40.47
34.51	0.20828	0 0 2	41.75
36.35	0.22366	1 0 1	39.08
47.64	0.24948	1 0 2	36.38
56.68	0.27027	1 1 0	34.91
62.93	0.30189	1 0 3	30.53
66.45	0.349	2 0 0	28.44
68.03	0.3221	1 1 2	31.10
69.18	0.3340	2 0 1	30.20

3.3. FESEM with EDS

The external morphology, topography, and particle size analyses of the phytogenic NPs were carried out by field emission scanning electron microscope. Fig. 2a and b represent the FESEM images of ZnO NPs of the study at different magnifications. From the images of FE-SEM, it could be observed the hexagonal shape of agglomerated morphology with the particle diameter in the range of about ~50 nm. These observations were confirmed by earlier reports of nanoparticles synthesized by biological routes (Jamdagni et al., 2018; Jayabalan et al., 2019). An individual cubic shaped ZnO nanostructure was observed in the FESEM image. The elemental composition of the ZnO NPs was studied by the EDS, which confirms the presence of metallic zinc oxide in phytogenic ZnO NPs (Ganesh et al., 2019; Vasantharaj et al., 2019). According to the EDX report, Fig. 2c reveals the predominant peaks representing the synthesized NPs atomic weight percentage of Zn and O were found to be 51.29 and 48.71% respectively in the synthesized nanoparticles. The higher composition of oxygen in NPs shows the fact that the prepared NPs are in oxide form. Aksu Demirezen et al. (2019) reported that the presence of a high amount of oxygen in the *Ficus carica* mediated iron oxide NPs suggest that the NPs are in iron oxide form. These two elements were higher in the percentage when compared with other elements, which arises from the reducing agents.

3.4. Ultra violet–visible absorption spectroscopy

The Ultra violet visible absorption spectroscopy was used for the analysis of optical properties of biologically synthesized ZnO NPs because this is the most widely used method for the characterization of nanoparticles. The UV–visible spectra of the synthesized ZnO NPs were shown in Fig. 3. The spectrum of synthesized ZnO NPs shows a strong absorption peak at 370 nm, which indicates the formation of ZnO NPs and no other absorption peak obtained in the visible range of 300–700 nm. This typical absorption edge falls at a lower wavelength or higher energy due to the decrease in the size of the ZnO NPs (Gupta et al., 2015). Also, a strong absorption peak at 370 nm which

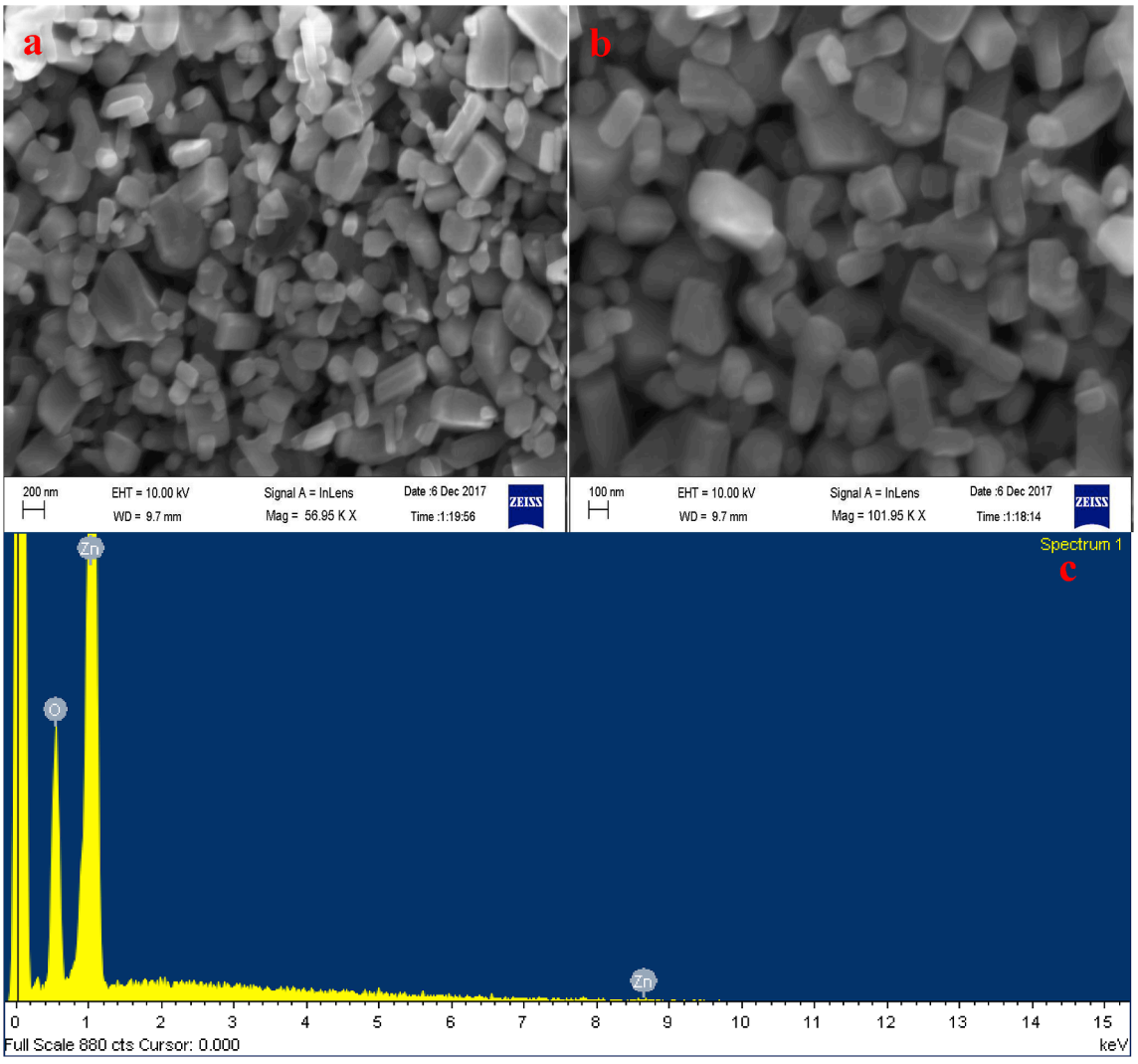

Fig. 2. FESEM micrograph of synthesized ZnO NPs and EDX spectrum (**a**). 200 nm scale, (**b**). 100 nm scale and (**c**). Elemental composition analysis.

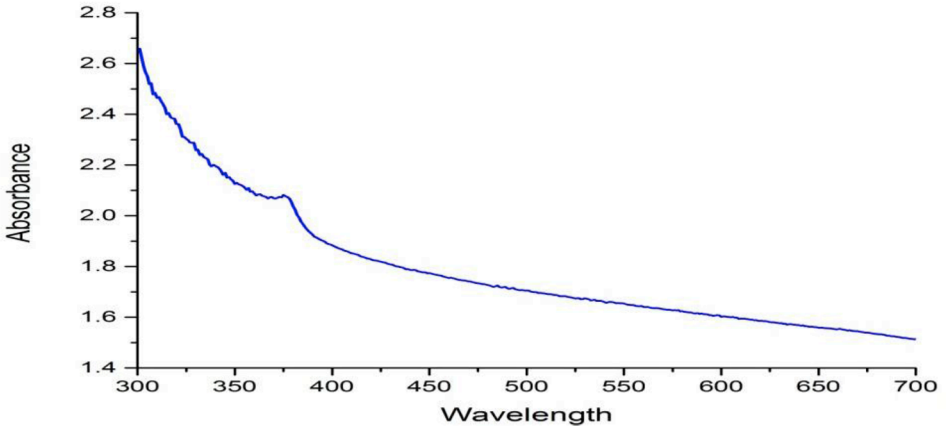

Fig. 3. UV–vis absorption spectra of ZnO NPs-synthesized by phytogenic method.

attributed to the intrinsic band-gap of ZnO due to the transitions of electrons from the valence band to the conduction band ($O_{2p} \rightarrow Zn_{3d}$) (Khorsand Zak et al., 2013). The as-prepared ZnO NPs solution shows a UV absorption edge shifting with respect to Zn materials. Efafi et al. (2013) and Šarić et al. (2019) reports, the precursor materials have significantly influenced the relationship between optical and particles size. This confirms the presence of ZnO NPs, which is in good agreement with the earlier reports (Jayabalan et al., 2019; Mohamed et al., 2019).

3.5. Dye degradation activity of ZnO NPs

Photocatalytic dye degradation activity of ZnO NPs was examined using the CV and MB under solar and UV light for different time intervals. The catalytic degradation of dyes in the presence of NPs was observed visually. The dye solution (without NPs) expressed no changes in absorption upon exposure to sunlight followed by UV-light, while the test solution having NPs with dye expressed a gradual decrease in absorbance. Fig. 4 shows the absorbance spectra of time-dependent degradation of CV and MB. A suitable concentration of NPs for CV/MB (0.5/1 and 2/3 mg) for solar and UV irradiation was found. Faster dye degradation occurred in the solar irradiation method in comparison to other irradiation methods with nanocatalyst (Panchal et al., 2019). The dye degradation percentage of CV/MB using ZnO NPs was calculated as 74.82/94.04 and 54.10/36.64% for sunlight and UV light irradiation respectively. Singh et al. (2019) reported that the catalytic activity of yellow dye (93.38%) was attributed to a wider band gap of phytogenic ZnO NPs. Generally, it is known that ZnO is a semi-

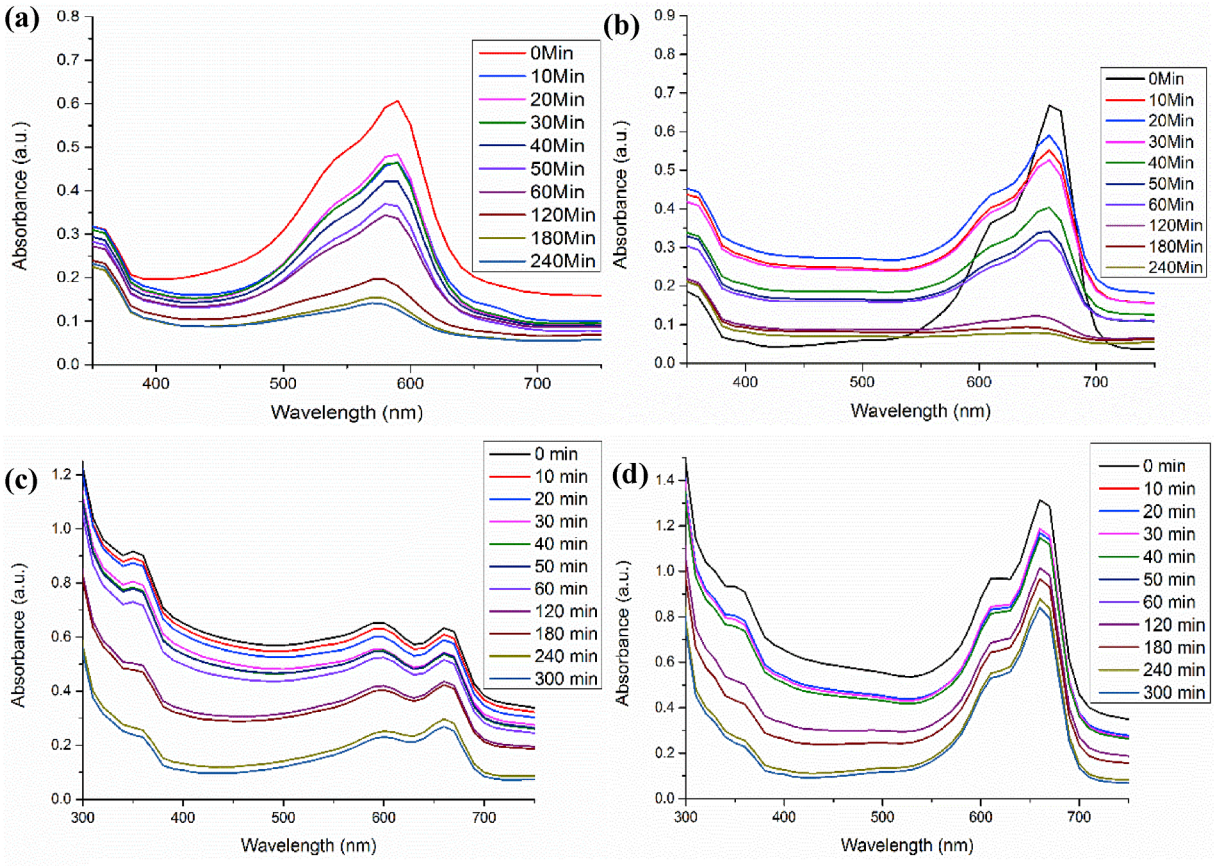

Fig. 4. Dye degradation activity of ZnO NPs. solar irradiation of CV and MB (**a** and **b**), UV irradiation of CV and MB (c and d).

conductor that has a conduction band (CB) valance band (VB) and electrons (e). These bands and electrons were produced by ZnO under solar, and UV illumination. The photons, and electrons are transferred from irradiated ZnO molecules and generate superoxide radical anion ($\bullet O^{-}_{2}$) and hydroxyl radicals (•OH) in the presence of water and O_2 molecules (Ahmed et al., 2017). The excited hydroxyl radical molecules further oxidize the dye pollutant molecules adsorbed by nanoparticles and degrade as its by-products (Khalafi et al., 2019). The results were comparable to similar studies that showed the time-dependent activity of nanomaterials is synthesized by various routes (Iqbal et al., 2019; Jaffri and Ahmad, 2018; Nagaraju et al., 2017; Zhang et al., 2018). Besides, recent studies reported that the photocatalytic activity could be strongly dependent on the shape, size of the nanoparticles, and a growth temperature (Hariharan et al., 2018; Li et al., 2014). This result indicates that the eco-friendly synthesized ZnO NPs have higher catalytic activity against CV and MB dyes compared with other reports.

3.6. Antipathogenic activity

Agar well diffusion method was employed in this study for antipathogenic activity assay to evaluate the efficacy of ZnO NPs against foodborne bacterial pathogens such as *Bacillus* sp., *E. coli*, *Staphylococcus aureus*, *Vibrio cholera*, *Corynebacterium* sp. and *Salmonella* sp. Streptomycin (10 μg/μL) was used as a positive control (PC), and the antimicrobial activity of ZnO NPs was evaluated by measuring the zone of inhibition. The observations demonstrate the antibacterial activity against all tested pathogens dose-dependently ($p < 0.05$). Fig. 5 and Table 2 shows the maximum zone of inhibition by NPs against bacterial pathogens. The antipathogenic activity of ZnO NPs mainly depends on the size and shape of the NPs (Li et al., 2010). The mechanism of the activity might be due to the release of Zn^{2+} ions into the bacterial cells by surface action of ZnO, resulting in cell membrane damage, leakage of cellular components, and eventually cell death (Kasemets et al., 2009; Li et al., 2008). Reactive oxygen species (ROS) (OH^{-}, H_2O_2, and O_2) is another co-factor for cell damage. Interaction between electron and hole with H_2O to produce $^{\bullet}OH$ and H^{+} ions, in addition O_2 molecules produce superoxide anion ($^{\bullet}O^{2-}$), which reacts with H^{+} and generates $HO^{\bullet}_{2}$. The generated $HO^{\bullet}_{2}$ interferes with elec-

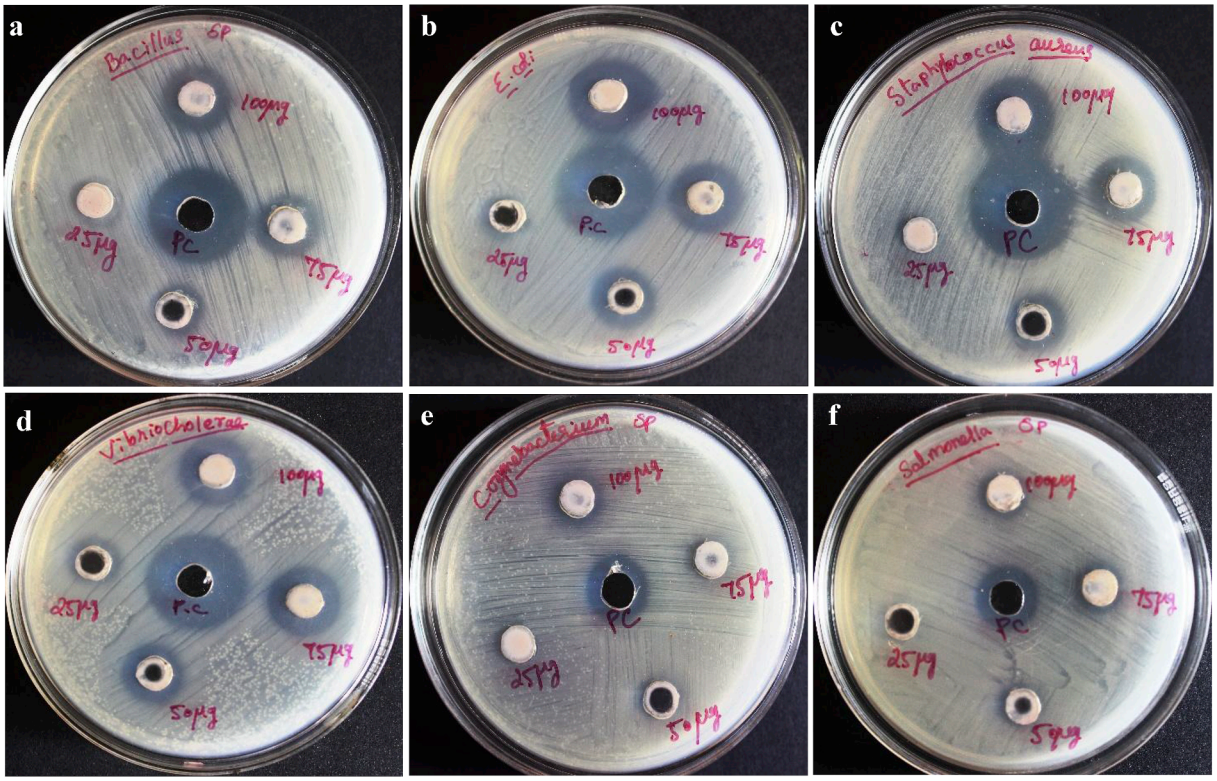

Fig. 5. Antibacterial activity of ZnO NPs against food borne pathogens of (**a**) *Bacillus* sp., (**b**) *E. coli*, (**c**) *Staphylococcus aureus*, (**d**) *Vibrio cholerea*, (**e**) *Corynebacterium* sp. and (**f**) *Salmonella* sp.

Table 2
Zone of inhibition of ZnO NPs at different concentrations. All the values are Mean ± SD of three replicates (Significant at $p < 0.05$)

Pathogens	Zone of Inhibition (mm)				
	Sterptomycin (μg/μL)	ZnO NPs concentration (μg/μL)			
	10	25	50	75	100
Bacillus sp.	21.00 ± 4.00^{a}	13.66 ± 2.08^{b}	17.00 ± 1.73^{ab}	17.33 ± 1.52^{ab}	20.33 ± 1.52^{a}
E. coli	21.00 ± 2.00^{a}	13.00 ± 2.00^{c}	16.33 ± 2.51^{bc}	18.33 ± 2.51^{b}	20.33 ± 1.52^{ab}
Staphylococcus aureus	24.66 ± 1.52^{a}	9.33. ± 3.51^{d}	15.66 ± 1.15^{c}	17.33 ± 1.52^{bc}	20.00 ± 1.00^{b}
Vibrio cholerae	23.33 ± 3.05^{a}	12.66 ± 1.52^{c}	15.66 ± 0.57^{bc}	16.33 ± 1.52^{b}	18.33 ± 0.57^{b}
Corynebacterium sp.	20.66 ± 4.04^{a}	9.33 ± 4.50^{b}	13.33 ± 3.78^{ab}	14.33 ± 3.78^{ab}	16.00 ± 3.46^{ab}
Salmonella sp.	19.00 ± 4.00^{a}	9.00 ± 3.00^{b}	14.00 ± 2.00^{a}	15.66 ± 1.52^{a}	17.00 ± 1.73^{a}

trons and produce hydrogen peroxide ($^{\bullet}HO_2$), which combines with H^+ and gives hydrogen peroxide (H_2O_2). These H_2O_2 molecules pass through the bacterial cell wall leading to death (Zhang et al., 2007). Previous studies report the mechanism of antibacterial activity is based on the generation of ROS from the surface of ZnO NPs resulting in oxidative stress to bacterial strains through DNA damage, as well as damage to the cell membrane and cellular proteins (Kadiyala et al., 2018; Tiwari et al., 2018).

3.7. In vitro cytotoxicity by MTT assay

In vitro cytotoxicity of ZnO NPs against A549 human lung cancer cell line was carried out by MTT assay. A549 cells were seeded in a 96 well culture plate, and cells were exposed to different concentrations (0–200 μg/mL) of ZnO NPs for 24 h. In this present study, the viability of A549 cells was decreased when the ZnO NPs concentration was increased and the IC_{50} value of ZnO NPs was found to be 51.25 ± 0.5 μg/mL (Fig. 6). The results show that there is a dose dependent cytotoxicity of ZnO NPs in treated cells (Surapaneni et al., 2018). Chung et al. (2015) reported similar dose-dependent cytotoxic activity of ZnO NPs on Hep-G2 cells. The cytotoxicity effects of nanoparticles on cells and tissues depend on the size, shape and cell type. The features such as induction of membrane leakage, DNA fragmentation and ability to activate the apoptotic mechanism by ROS generation of ZnO NPs treated cells were due to the toxic effects of NPs (Prashanth et al., 2015). Several studies reveals that certain metal oxide nanomaterials potentially exhibit the ROS spontaneously based on the composition and surface of the nanoparticles (Long et al., 2006; Xia et al., 2006).

3.8. AO/EB dual staining

To examine the morphology, antiproliferative and cytotoxic effects of NPs besides the assessment of apoptosis induced by NPs in A549 cells, the cells after treatment were stained with AO/EB. The cells were treated, based on the acquired IC_{50} concentration of NPs and stained with AO/EB, followed by observation under a fluorescent microscope. Fig. 7a shows the normal nuclei of untreated cells (control) and their intact shape. ZnO NPs treated cells showed (Fig. 7b) apoptotic bodies and other apoptotic features such as cell shrinkage, chromatin condensation, necrosis and fragmented nuclei (Ho et al., 2009). Oxidative stress is the most argued paradigm for the cytotoxicity of oxide NPs, which can be attributed by the small size and large surface area. These properties generally produce ROS and oxidative stress (Xia et al., 2006). Sharma et al. (2012) proposed the mechanism of ZnO NPs cytotoxicity of human liver cells (HepG2) and that cell death was mediated by apoptosis, which triggers the ROS. These results suggest that ZnO NPs effectively induced apoptosis in treated cancer cell lines.

3.9. Nuclear staining

Hoechst 33258 is widely used to stain the nuclei of both the healthy and dead cells, especially when the DNA of apoptotic cells were in condensed state; however, this distinct feature is not known to occur during necrosis (Zhivotosky and Orrenius, 2001). The untreated control A549 cells (Fig. 7c) showed normal nuclei when viewed using fluorescence microscope. Nuclear staining of treated cells shows distinguished apoptotic changes including the features such as chromatin condensation, nuclear fragmentation and abnormal nuclei when the cells are treated with respect to the inhibitory concentration (Fig. 7d). A previous report (Bai Aswathanarayan et al., 2018) shows that the cytotoxicity effects of different metal oxide nanoparticles suggest that the apoptosis has to be the major mechanism for the cell death, especially ZnO NPs has more cytotoxic activity compared with other NPs. This result suggests that the exposure of ZnO NPs could induce apoptosis in A549 cell line.

3.10. Mitochondrial membrane potential (Δψm)

Mitochondria play a crucial role in providing energy for cell survival by means of synthesizing ATP. The intactness or functional integrity of mitochondria is essential for cell survival and is determined by mitochondrial membrane potential (Δψm). Results of the mitochondrial membrane potential analysis showed that Δψm decreased when the cells were treated with IC_{50} concentration of phytogenic ZnO NPs. Rhodamine 123 is a cell-permeable fluorescent dye, which enters into mitochondria of live cells. As shown in Fig. 7e, the control cells emit green fluorescence at a high intensity of A549 cell, whereas the treated cells show the depleted fluorescence (Fig. 7f) revealing the loss of mitochondrial membrane integrity of cells treated with ZnO NPs. The loss of Δψm could be due to the generation of ROS through oxidative stress originated in treated cells altering the levels of ATP resulting in cell death (Maity et al., 2018; Surapaneni et al., 2018).

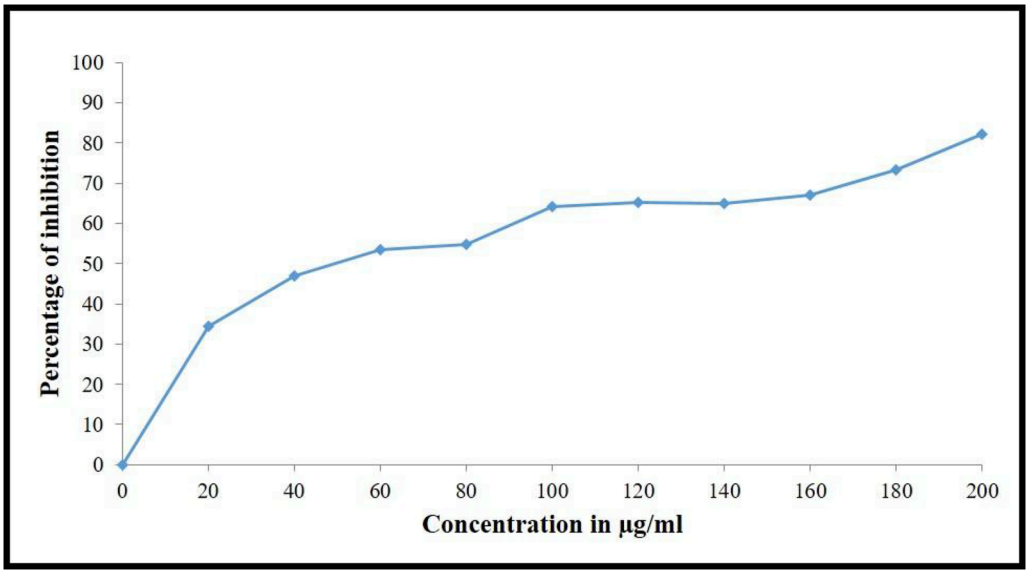

Fig. 6. *In vitro* cytotoxicity effects of phytogenic ZnO NPs on human lung cancer A549 cell lines analysed by MTT assay.

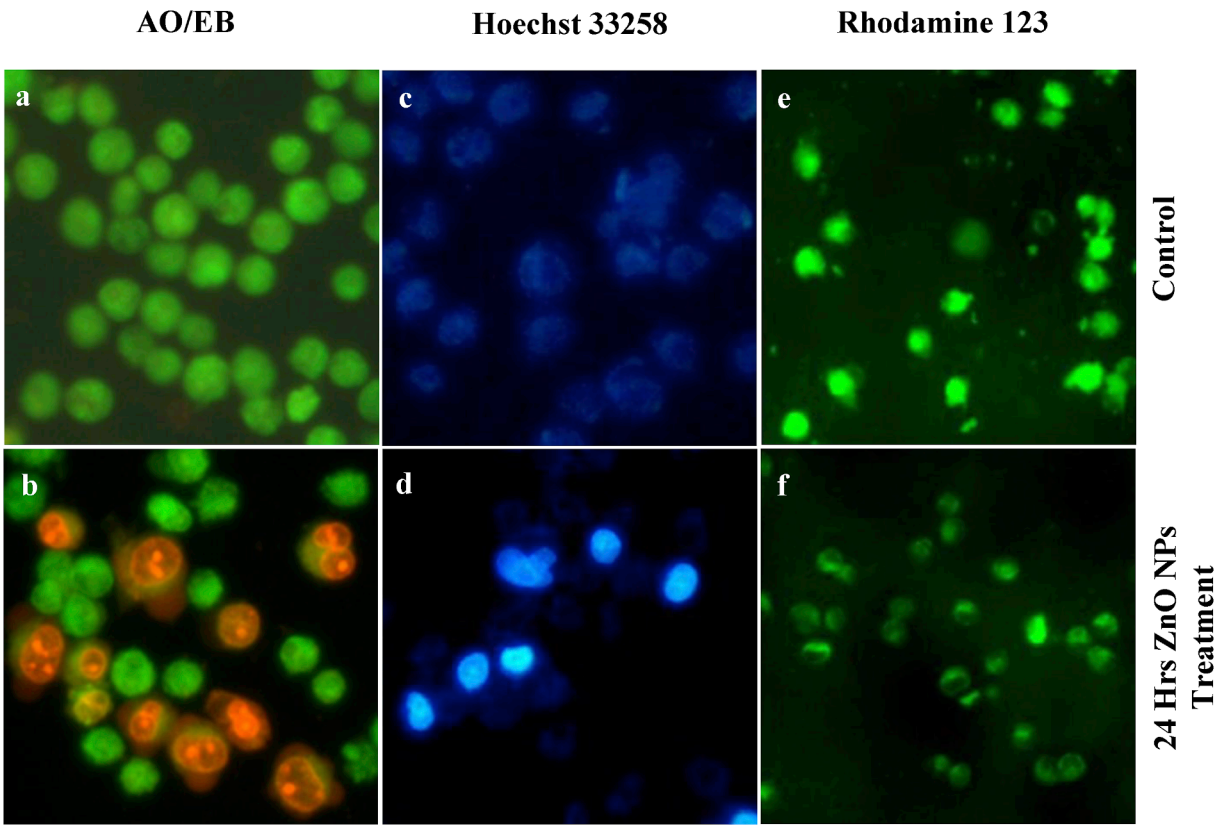

Fig. 7. Fluorescent microscope images of 24 h ZnO NPs treated A549 cell line (**a** and **b)** Ao/EtBr staining, (**c** and **d**) Hoechst 33258 staining, (**e** and **f**) Rhodamine 123 staining.

3.11. Cell cycle analysis

PI staining was used to evaluate the cell cycle distribution of control and ZnO NPs treated A459 cells (Fig. 8) by flow cytometry. ZnO NPs treated cells showed cell cycle profile with significantly increased cell cycle arrest was found in the sub-G_1 and S phase compared to control cells. Most of the cells were arrested at the G_1 and S phases, and a complete arrest was found at the G_2 phase. These results suggested that the inhibition of cell growth was reduced due to Sub-G_1 phase arrest resulting in the induction of apoptosis. ZnO NPs could exhibit cell cycle arrest in various phases but the extent may vary from one phase to another. The ZnO NPs induced apoptosis was due to ROS generation, chromatin condensation, cell shrinkage and fragmentation of nuclei (Zhang et al., 2013).

4. Conclusion

The study about the formulation of ZnO NPs from dried onion peels, which are usually regarded as waste material is a new research topic. The synthesized ZnO NPs were characterized using various ana-

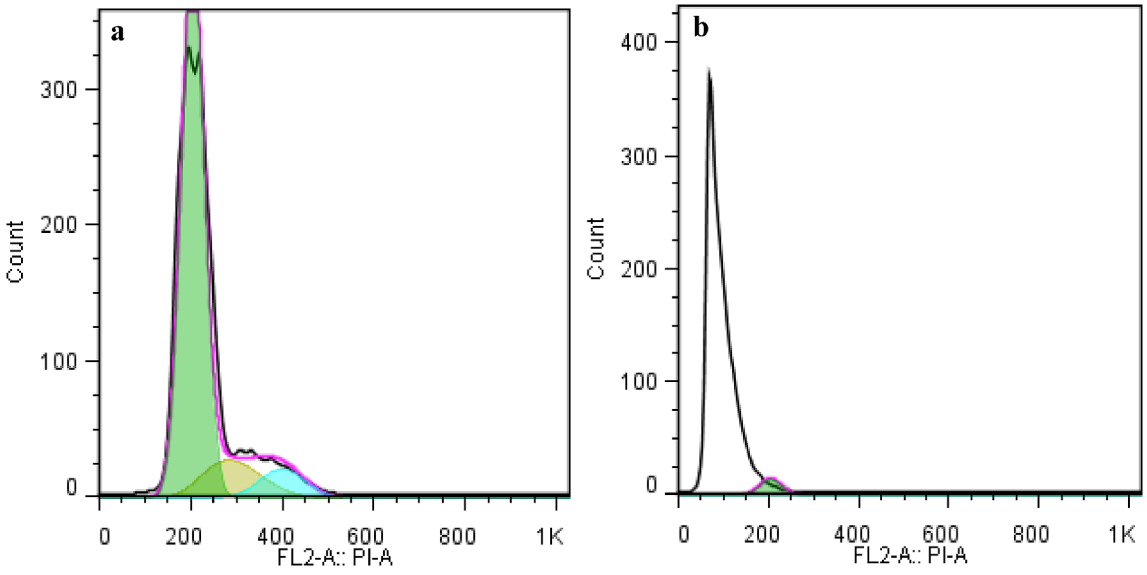

Fig. 8. Flow cytometry analysis of A549 cells. (**a**) Control and (**b**) ZnO NPs treated cells investigated after PI staining.

lytical tools. Phytogenic ZnO NPs showed excellent photocatalytic activity in the degradation of CV and MB dyes. The synthesized NPs displayed less toxicity as shown by *in vitro* studies. Further, the efficiency of antipathogenic activity of ZnO NPs against foodborne bacterial pathogens at low concentration substantiates the potential of the synthesized NPs. It could be used as an effective therapeutic option along with the conventional antibiotics. As the study ZnO NPs are synthesized using waste phytoproducts, the study envisages a paradigm shift in the nanosynthesis by means of waste to wealth generation due to its promising biomedical applications.

Acknowledgement

The author K.S. Rajkumar gratefully acknowledges the Department of Science & Technology (DST), Govt. of India for providing fellowship under the INSPIRE Fellowship (IF140546). The authors thank UGC-CPEPA National Centre for Alternatives to Animal Experiments for cell culture studies in this work. The authors are grateful to UGC-SAP DRS-II and DST FIST-II for providing instrumentation facilities in the Department of Animal Science, Bharathidasan University, Tiruchirappalli, Tamil Nadu, India.

Appendix A. Supplementary data

Supplementary data to this article can be found online at https://doi.org/10.1016/j.bcab.2019.101436.

References

Ahmed, S., Annu Chaudhry, S.A., Ikram, S., 2017. A review on biogenic synthesis of ZnO nanoparticles using plant extracts and microbes: a prospect towards green chemistry. J. Photochem. Photobiol. B Biol.. https://doi.org/10.1016/j.jphotobiol.2016.12.011.

Aksu Demirezen, D., Yıldız, Y.Ş., Yılmaz, Ş., Demirezen Yılmaz, D., 2019. Green synthesis and characterization of iron oxide nanoparticles using Ficus carica (common fig) dried fruit extract. J. Biosci. Bioeng.. https://doi.org/10.1016/j.jbiosc.2018.07.024.

Al Abdullah, K., Awad, S., Zaraket, J., Salame, C., 2017. Synthesis of ZnO nanopowders by using sol-gel and studying their structural and electrical properties at different temperature. Energy Procedia. https://doi.org/10.1016/j.egypro.2017.07.080.

Ali, M., Thomson, M., Afzal, M., 2000. Garlic and onions: their effect on eicosanoid metabolism and its clinical relevance. Prostaglandins Leukot. Essent. Fatty Acids. https://doi.org/10.1054/plef.1999.0124.

Ambika, S., Sundrarajan, M., 2015. Antibacterial behaviour of Vitex negundo extract assisted ZnO nanoparticles against pathogenic bacteria. J. Photochem. Photobiol. B Biol.. https://doi.org/10.1016/j.jphotobiol.2015.02.020.

Bai Aswathanarayan, J., Rai Vittal, R., Muddegowda, U., 2018. Anticancer activity of metal nanoparticles and their peptide conjugates against human colon adenorectal carcinoma cells. Artif. Cells Nanomed. Biotechnol.. https://doi.org/10.1080/21691401.2017.1373655.

Baracca, A., Sgarbi, G., Solaini, G., Lenaz, G., 2003. Rhodamine 123 as a probe of mitochondrial membrane potential: evaluation of proton flux through F0 during ATP synthesis. Biochim. Biophys. Acta Bioenerg.. https://doi.org/10.1016/S0005-2728(03)00110-5.

Cai, L., Chen, J., Liu, Z., Wang, H., Yang, H., Ding, W., 2018. Magnesium oxide nanoparticles: effective agricultural antibacterial agent against Ralstonia solanacearum. Front. Microbiol.. https://doi.org/10.3389/fmicb.2018.00790.

Chung, I.M., Rahuman, A.A., Marimuthu, S., Kirthi, A.V., Anbarasan, K., Rajakumar, G., 2015. An investigation of the cytotoxicity and caspase-mediated apoptotic effect of green synthesized zinc oxide nanoparticles using Eclipta prostrata on human liver carcinoma cells. Nanomaterials 5, 1317–1330. https://doi.org/10.3390/nano5031317.

Cullity, B.D., Stock, S.R., 2001. Elements of X-Ray Diffraction. Prentice hall, New Jersey.

Darroudi, M., Sabouri, Z., Kazemi Oskuee, R., Khorsand Zak, A., Kargar, H., Abd Hamid, M.H.N., 2014. Green chemistry approach for the synthesis of ZnO nanopowders and their cytotoxic effects. Ceram. Int.. https://doi.org/10.1016/j.ceramint.2013.09.032.

Dobrucka, R., Długaszewska, J., 2016. Biosynthesis and antibacterial activity of ZnO nanoparticles using Trifolium pratense flower extract. Saudi J. Biol. Sci.. https://doi.org/10.1016/j.sjbs.2015.05.016.

Dzul-Erosa, M.S., Cauich-Díaz, M.M., Razo-Lazcano, T.A., Avila-Rodriguez, M., Reyes-Aguilera, J.A., González-Muñoz, M.P., 2018. Aqueous leaf extracts of Cnidoscolus chayamansa (Mayan chaya) cultivated in Yucatán México. Part II: uses for the phytomediated synthesis of silver nanoparticles. Mater. Sci. Eng. C. https://doi.org/10.1016/j.msec.2018.06.007.

Efafi, B., Sasani Ghamsari, M., Aberoumand, M.A., Majles Ara, M.H., Hojati Rad, H., 2013. Highly concentrated ZnO sol with ultra-strong green emission. Mater. Lett.. https://doi.org/10.1016/j.matlet.2013.08.035.

Elnima, E.I., Ahmed, S.A., Mekkawi, A.G., Mossa, J.S., 1983. The antimicrobial activity of garlic and onion extracts. Die Pharmazie 38, 747–748.

Fakhari, S., Jamzad, M., Kabiri Fard, H., 2019. Green synthesis of zinc oxide nanoparticles: a comparison. Green Chem. Lett. Rev. 12, 19–24. https://doi.org/10.1080/17518253.2018.1547925.

Ganesh, M., Lee, S.G., Jayaprakash, J., Mohankumar, M., Jang, H.T., 2019. Hydnocarpus alpina Wt extract mediated green synthesis of ZnO nanoparticle and screening of its anti-microbial, free radical scavenging, and photocatalytic activity. Biocatal. Agric. Biotechnol.. https://doi.org/10.1016/j.bcab.2019.101129.

Gnanasekaran, L., Hemamalini, R., Saravanan, R., Ravichandran, K., Gracia, F., Agarwal, S., Gupta, V.K., 2017. Synthesis and characterization of metal oxides (CeO2, CuO, NiO, Mn3O4, SnO2 and ZnO) nanoparticles as photo catalysts for degradation of textile dyes. J. Photochem. Photobiol. B Biol.. https://doi.org/10.1016/j.jphotobiol.2017.05.027.

Gupta, A., Srivastava, P., Bahadur, L., Amalnerkar, D.P., Chauhan, R., 2015. Comparison of physical and electrochemical properties of ZnO prepared via different surfactant-assisted precipitation routes. Appl. Nanosci.. https://doi.org/10.1007/s13204-014-0379-1.

Hariharan, D., Jegatha Christy, A., Mayandi, J., Nehru, L.C., 2018. Visible light active photocatalyst: hydrothermal green synthesized TiO2 NPs for degradation of picric acid. Mater. Lett. 222, 45–49. https://doi.org/10.1016/j.matlet.2018.03.109.

Hassan, S.S.M., Azab, W.I.M.E., Ali, H.R., Mansour, M.S.M., 2015. Green synthesis and characterization of ZnO nanoparticles for photocatalytic degradation of anthracene. Adv. Nat. Sci. Nanosci. Nanotechnol.. https://doi.org/10.1088/2043-6262/6/4/045012.

Ho, K.L., Yazan, L.S., Ismail, N., Ismail, M., 2009. Apoptosis and cell cycle arrest of human colorectal cancer cell line HT-29 induced by vanillin. Cancer Epidemiol.. https://doi.org/10.1016/j.canep.2009.06.003.

Hoseinnejad, M., Jafari, S.M., Katouzian, I., 2018. Inorganic and metal nanoparticles and their antimicrobial activity in food packaging applications. Crit. Rev. Microbiol.. https://doi.org/10.1080/1040841X.2017.1332001.

Iqbal, J., Abbasi, B.A., Mahmood, T., Hameed, S., Munir, A., Kanwal, S., 2019. Green synthesis and characterizations of Nickel oxide nanoparticles using leaf extract of Rhamnus virgata and their potential biological applications. Appl. Organomet. Chem.. https://doi.org/10.1002/aoc.4950.

Jaffri, S.B., Ahmad, K.S., 2018. Augmented photocatalytic, antibacterial and antifungal activity of prunosynthetic silver nanoparticles. Artif. Cells Nanomed. Biotechnol. 46, 127–137. https://doi.org/10.1080/21691401.2017.1414826.

Jamdagni, P., Khatri, P., Rana, J.S., 2018. Green synthesis of zinc oxide nanoparticles using flower extract of Nyctanthes arbor-tristis and their antifungal activity. J. King Saud Univ. Sci.. https://doi.org/10.1016/j.jksus.2016.10.002.

Jamdagni, P., Khatri, P., Rana, J.S., 2016. Green synthesis of zinc oxide nanoparticles using flower extract of Nyctanthes arbor-tristis and their antifungal activity. J. King Saud Univ. Sci. 30. https://doi.org/10.1016/j.jksus.2016.10.002.

Jayabalan, J., Mani, G., Krishnan, N., Pernabas, J., Devadoss, J.M., Jang, H.T., 2019. Green biogenic synthesis of zinc oxide nanoparticles using Pseudomonas putida culture and its in vitro antibacterial and anti-biofilm activity. Biocatal. Agric. Biotechnol.. https://doi.org/10.1016/j.bcab.2019.101327.

Kadiyala, U., Turali-Emre, E.S., Bahng, J.H., Kotov, N.A., Scott Vanepps, J., 2018. Unexpected insights into antibacterial activity of zinc oxide nanoparticles against methicillin resistant: Staphylococcus aureus (MRSA). Nanoscale. https://doi.org/10.1039/c7nr08499d.

Kasemets, K., Ivask, A., Dubourguier, H.C., Kahru, A., 2009. Toxicity of nanoparticles of ZnO, CuO and TiO2 to yeast Saccharomyces cerevisiae. Toxicol. In Vitro. https://doi.org/10.1016/j.tiv.2009.05.015.

Kasibhatla, S., 2006. Staining of suspension cells with Hoechst 33258 to detect apoptosis. Cold Spring Harb. Protoc.. https://doi.org/10.1101/pdb.prot4492.

Khalafi, T., Buazar, F., Ghanemi, K., 2019. Phycosynthesis and enhanced photocatalytic activity of zinc oxide nanoparticles toward organosulfur pollutants. Sci. Rep.. https://doi.org/10.1038/s41598-019-43368-3.

Khalil, A.T., Ovais, M., Ullah, I., Ali, M., Shinwari, Z.K., Hassan, D., Maaza, M., 2018. Sageretia thea (Osbeck.) modulated biosynthesis of NiO nanoparticles and their in vitro pharmacognostic, antioxidant and cytotoxic potential. Artif. Cells Nanomed. Biotechnol.. https://doi.org/10.1080/21691401.2017.1345928.

Khalilzadeh, M.A., Borzoo, M., 2016. Green synthesis of silver nanoparticles using onion extract and their application for the preparation of a modified electrode for determination of ascorbic acid. J. Food Drug Anal.. https://doi.org/10.1016/j.jfda.2016.05.004.

Khan, Z.U.H., Sadiq, H.M., Shah, N.S., Khan, A.U., Muhammad, N., Hassan, S.U., Tahir, K., safi, S.Z., Khan, F.U., Imran, M., Ahmad, N., Ullah, F., Ahmad, A., Sayed, M., Khalid, M.S., Qaisrani, S.A., Ali, M., Zakir, A., 2019. Greener synthesis of zinc oxide nanoparticles using Trianthema portulacastrum extract and evaluation of its photocatalytic and biological applications. J. Photochem. Photobiol. B Biol. 192, 147–157. https://doi.org/10.1016/j.jphotobiol.2019.01.013.

Khorsand Zak, A., Abd Majid, W.H., Mahmoudian, M.R., Darroudi, M., Yousefi, R., 2013. Starch-stabilized synthesis of ZnO nanopowders at low temperature and optical properties study. Adv. Powder Technol.. https://doi.org/10.1016/j.apt.2012.11.008.

Kim, J., Cha, Y.J., Lee, K.H., Park, E., 2013. Effect of onion peel extract supplementation on the lipid profile and antioxidative status of healthy young women: a randomized, placebo-controlled, double-blind, crossover trial. Nutr. Res. Pract.. https://doi.org/10.4162/nrp.2013.7.5.373.

Li, Q., Mahendra, S., Lyon, D.Y., Brunet, L., Liga, M.V., Li, D., Alvarez, P.J.J., 2008. Antimicrobial nanomaterials for water disinfection and microbial control: potential applications and implications. Water Res.. https://doi.org/10.1016/j.watres.2008.

08.015.
Li, W.R., Xie, X.B., Shi, Q.S., Zeng, H.Y., Ou-Yang, Y.S., Chen, Y.B., 2010. Antibacterial activity and mechanism of silver nanoparticles on Escherichia coli. Appl. Microbiol. Biotechnol.. https://doi.org/10.1007/s00253-009-2159-5.
Long, T.C., Saleh, N., Tilton, R.D., Lowry, G.V., Veronesi, B., 2006. Titanium dioxide (P25) produces reactive oxygen species in immortalized brain microglia (BV2): implications for nanoparticle neurotoxicity. Environ. Sci. Technol. 40, 4346–4352. https://doi.org/10.1021/es060589n.
Ma, H., Williams, P.L., Diamond, S.A., 2013. Ecotoxicity of manufactured ZnO nanoparticles - a review. Environ. Pollut.. https://doi.org/10.1016/j.envpol.2012.08.011.
Maity, P., Bepari, M., Pradhan, A., Baral, R., Roy, S., Maiti Choudhury, S., 2018. Synthesis and characterization of biogenic metal nanoparticles and its cytotoxicity and anti-neoplasticity through the induction of oxidative stress, mitochondrial dysfunction and apoptosis. Colloids Surfaces B Biointerfaces. https://doi.org/10.1016/j.colsurfb.2017.10.040.
Malakootian, M., Gharaghani, M.A., Dehdarirad, A., Khatami, M., Ahmadian, M., Heidari, M.R., Mahdizadeh, H., 2019. ZnO nanoparticles immobilized on the surface of stones to study the removal efficiency of 4-nitroaniline by the hybrid advanced oxidation process (UV/ZnO/O3). J. Mol. Struct.. https://doi.org/10.1016/j.molstruc.2018.09.033.
Mayedwa, N., Mongwaketsi, N., Khamlich, S., Kaviyarasu, K., Matinise, N., Maaza, M., 2018. Green synthesis of zin tin oxide (ZnSnO3) nanoparticles using Aspalathus Linearis natural extracts: structural, morphological, optical and electrochemistry study. Appl. Surf. Sci.. https://doi.org/10.1016/j.apsusc.2017.12.161.
Mhaskar, K.S., Blatter, E., Caius, J.F., Ram, V.A., 2000. Kirtikar and Basu's Illustrated Indian Medicinal Plants : Their Usage in Ayurveda and Unani Medicines, vol. 1. Sri Satguru Publications, Delhi.
Miri, A., Mahdinejad, N., Ebrahimy, O., Khatami, M., Sarani, M., 2019. Zinc oxide nanoparticles: biosynthesis, characterization, antifungal and cytotoxic activity. Mater. Sci. Eng. C. https://doi.org/10.1016/j.msec.2019.109981.
Mohamed, A.A., Fouda, A., Abdel-Rahman, M.A., Hassan, S.E.D., El-Gamal, M.S., Salem, S.S., Shaheen, T.I., 2019. Fungal strain impacts the shape, bioactivity and multifunctional properties of green synthesized zinc oxide nanoparticles. Biocatal. Agric. Biotechnol.. https://doi.org/10.1016/j.bcab.2019.101103.
Mosmann, T., 1983. Rapid colorimetric assay for cellular growth and survival: application to proliferation and cytotoxicity assays. J. Immunol. Methods. https://doi.org/10.1016/0022-1759(83)90303-4.
Nagaraju, G., Shivaraju, G.C., Banuprakash, G., Rangappa, D., 2017. Photocatalytic activity of ZnO nanoparticles: synthesis via solution combustion method. Mater. Today Proc. 4, 11700–11705. https://doi.org/10.1016/j.matpr.2017.09.085.
Nasrollahzadeh, M., Sajjadi, M., Komber, H., Khonakdar, H.A., Sajadi, S.M., 2019. In situ green synthesis of Cu-Ni bimetallic nanoparticles supported on reduced graphene oxide as an effective and recyclable catalyst for the synthesis of N-benzyl-N-aryl-5-amino-1H-tetrazoles. Appl. Organomet. Chem. 33, e4938. https://doi.org/10.1002/aoc.4938.
Ovais, M., Zia, N., Ahmad, I., Khalil, A.T., Raza, A., Ayaz, M., Sadiq, A., Ullah, F., Shinwari, Z.K., 2018. Phyto-therapeutic and nanomedicinal approaches to cure Alzheimer's disease: present status and future opportunities. Front. Aging Neurosci. 10, 284. https://doi.org/10.3389/fnagi.2018.00284.
Panchal, P., Paul, D.R., Sharma, A., Hooda, D., Yadav, R., Meena, P., Nehra, S.P., 2019. Phytoextract mediated ZnO/MgO nanocomposites for photocatalytic and antibacterial activities. J. Photochem. Photobiol. A Chem. 385, 112049. https://doi.org/10.1016/j.jphotochem.2019.112049.
Prakash, D., Singh, B.N., Upadhyay, G., 2007. Antioxidant and free radical scavenging activities of phenols from onion (Allium cepa). Food Chem.. https://doi.org/10.1016/j.foodchem.2006.06.063.
Prasad, A.S., 2014. Zinc is an antioxidant and anti-inflammatory agent: its role in human health. Front. Nutr.. https://doi.org/10.3389/fnut.2014.00014.
Prashanth, G.K., Prashanth, P.A., Utpal, B., Gadewar, M., Nagabhushana, B.M., Ananda, S., Krishnaiah, G.M., Sathyananda, H.M., 2015. In vitro antibacterial and cytotoxicity studies of ZnO nanopowders prepared by combustion assisted facile green synthesis. Karbala Int. J. Mod. Sci. https://doi.org/10.1016/j.kijoms.2015.10.007.
Pugazhendhi, A., Edison, T.N.J.I., Karuppusamy, I., Kathirvel, B., 2018. Inorganic nanoparticles: a potential cancer therapy for human welfare. Int. J. Pharm.. https://doi.org/10.1016/j.ijpharm.2018.01.034.
Pugazhendhi, A., Kumar, S.S., Manikandan, M., Saravanan, M., 2018. Photocatalytic properties and antimicrobial efficacy of Fe doped CuO nanoparticles against the pathogenic bacteria and fungi. Microb. Pathog.. https://doi.org/10.1016/j.micpath.2018.06.016.
Pugazhendhi, A., Prabakar, D., Jacob, J.M., Karuppusamy, I., Saratale, R.G., 2018. Synthesis and characterization of silver nanoparticles using Gelidium amansii and its antimicrobial property against various pathogenic bacteria. Microb. Pathog.. https://doi.org/10.1016/j.micpath.2017.11.013.
Pugazhendhi, A., Prabhu, R., Muruganantham, K., Shanmuganathan, R., Natarajan, S., 2019. Anticancer, antimicrobial and photocatalytic activities of green synthesized magnesium oxide nanoparticles (MgONPs) using aqueous extract of Sargassum wightii. J. Photochem. Photobiol. B Biol.. https://doi.org/10.1016/j.jphotobiol.2018.11.014.
Rahman, S., Rahman, L., Khalil, A.T., Ali, N., Zia, D., Ali, M., Shinwari, Z.K., 2019. Endophyte-mediated synthesis of silver nanoparticles and their biological applications. Appl. Microbiol. Biotechnol.. https://doi.org/10.1007/s00253-019-09661-x.
Rajkumar, K.S., Kanipandian, N., Thirumurugan, R., 2016. Toxicity assessment on haemotology, biochemical and histopathological alterations of silver nanoparticles-exposed freshwater fish Labeo rohita. Appl. Nanosci.. https://doi.org/10.1007/s13204-015-0417-7.
Rasmussen, J.W., Martinez, E., Louka, P., Wingett, D.G., 2010. Zinc oxide nanoparticles for selective destruction of tumor cells and potential for drug delivery applications. Expert Opin. Drug Deliv.. https://doi.org/10.1517/17425247.2010.502560.
Rodrigues, T.S., da Silva, A.G.M., Camargo, P.H.C., 2019. Nanocatalysis by noble metal nanoparticles: controlled synthesis for the optimization and understanding of activities. J. Mater. Chem. 7, 5857–5874. https://doi.org/10.1039/C9TA00074G.
Saha, J., Begum, A., Mukherjee, A., Kumar, S., 2017. A novel green synthesis of silver nanoparticles and their catalytic action in reduction of Methylene Blue dye. Sustain. Environ. Res.. https://doi.org/10.1016/j.serj.2017.04.003.
Sahni, G., Panwar, A., Kaur, B., 2015. Controlled green synthesis of silver nanoparticles by *Allium cepa* and *Musa acuminata* with strong antimicrobial activity. Int. Nano Lett.. https://doi.org/10.1007/s40089-015-0142-y.
Sakakibara, H., Yoshino, S., Kawai, Y., Terao, J., 2008. Antidepressant-like effect of onion (Allium cepa L.) powder in a rat behavioral model of depression. Biosci. Biotechnol. Biochem.. https://doi.org/10.1271/bbb.70454.
Saratale, R.G., Ghodake, G.S., Shinde, S.K., Cho, S.-K., Saratale, G.D., Pugazhendhi, A., Bharagava, R.N., 2018. Photocatalytic activity of CuO/Cu(OH)2 nanostructures in the degradation of Reactive Green 19A and textile effluent, phytotoxicity studies and their biogenic properties (antibacterial and anticancer). J. Environ. Manag. 223, 1086–1097. https://doi.org/10.1016/j.jenvman.2018.04.072.
Šarić, A., Despotović, I., Štefanić, G., 2019. Solvothermal synthesis of zinc oxide nanoparticles: a combined experimental and theoretical study. J. Mol. Struct.. https://doi.org/10.1016/j.molstruc.2018.10.025.
Šarić, A., Despotović, I., Štefanić, G., Dražić, G., 2017. The influence of ethanolamines on the solvothermal synthesis of zinc oxide: a combined experimental and theoretical study. ChemistrySelect 2, 10038–10049. https://doi.org/10.1002/slct.201701692.
Seabra, N.D.*, Seabra, A.B., 2018. Biogenic synthesized Ag/Au nanoparticles: production, characterization, and applications. Curr. Nanosci.. https://doi.org/10.2174/1573413714666171207160637.
Senthilkumar, S.R., Sivakumar, T., 2014. Green tea (Camellia sinensis) mediated synthesis of zinc oxide (ZnO) nanoparticles and studies on their antimicrobial activities. Int. J. Pharm. Pharm. Sci..
Shah, A., Lutfullah, G., Ahmad, K., Khalil, A.T., Maaza, M., 2018. Daphne mucronata-mediated phytosynthesis of silver nanoparticles and their novel biological applications, compatibility and toxicity studies. Green Chem. Lett. Rev. 11, 318–333. https://doi.org/10.1080/17518253.2018.1502365.
Sharma, V., Anderson, D., Dhawan, A., 2012. Zinc oxide nanoparticles induce oxidative DNA damage and ROS-triggered mitochondria mediated apoptosis in human liver cells (HepG2). Apoptosis. https://doi.org/10.1007/s10495-012-0705-6.
Siegel, R., Ma, J., Zou, Z., Jemal, A., 2014. Cancer statistics, 2014. CA. Cancer J. Clin. 64, 9–29. https://doi.org/10.3322/caac.21208.
Singh, J., Kaur, S., Kaur, G., Basu, S., Rawat, M., 2019. Biogenic ZnO nanoparticles: a study of blueshift of optical band gap and photocatalytic degradation of reactive yellow 186 dye under direct sunlight. Green Process. Synth.. https://doi.org/10.1515/gps-2018-0084.
Spector, D.L., Goldman, R.D., Leinwand, L.A., 1998. Cells : a Laboratory Manual, vol. 1. Cold Spring Harbor Laboratory Press, Plainview, N.Y Volume 1,.
Stan, M., Popa, A., Toloman, D., Dehelean, A., Lung, I., Katona, G., 2015. Enhanced photocatalytic degradation properties of zinc oxide nanoparticles synthesized by using plant extracts. Mater. Sci. Semicond. Process.. https://doi.org/10.1016/j.mssp.2015.04.038.
Sukhanova, A., Bozrova, S., Sokolov, P., Berestovoy, M., Karaulov, A., Nabiev, I., 2018. Dependence of nanoparticle toxicity on their physical and chemical properties. Nanoscale Res. Lett.. https://doi.org/10.1186/s11671-018-2457-x.
Sun, T., Zhang, Y.S., Pang, B., Hyun, D.C., Yang, M., Xia, Y., 2014. Engineered nanoparticles for drug delivery in cancer therapy. Angew. Chem. Int. Ed.. https://doi.org/10.1002/anie.201403036.
Surapaneni, S.K., Bashir, S., Tikoo, K., 2018. Gold nanoparticles-induced cytotoxicity in triple negative breast cancer involves different epigenetic alterations depending upon the surface charge. Sci. Rep.. https://doi.org/10.1038/s41598-018-30541-3.
Li, X., Guo, W., Huang, H., Chen, T., Zhang, M., Wang, Y., 2014. Synthesis and Photocatalytic properties of CuO nanostructures. J. Nanosci. Nanotechnol. 14.
Tiwari, V., Mishra, N., Gadani, K., Solanki, P.S., Shah, N.A., Tiwari, M., 2018. Mechanism of anti-bacterial activity of zinc oxide nanoparticle against Carbapenem-Resistant Acinetobacter baumannii. Front. Microbiol.. https://doi.org/10.3389/fmicb.2018.01218.
Vasantharaj, S., Sathiyavimal, S., Saravanan, M., Senthilkumar, P., Gnanasekaran, K., Shanmugavel, M., Manikandan, E., Pugazhendhi, A., 2019. Synthesis of ecofriendly copper oxide nanoparticles for fabrication over textile fabrics: characterization of antibacterial activity and dye degradation potential. J. Photochem. Photobiol. B Biol.. https://doi.org/10.1016/j.jphotobiol.2018.12.026.
Wang, Z., Xie, C., Huang, Y., Lam, C.W.K., Chow, M.S.S., 2014. Overcoming chemotherapy resistance with herbal medicines: past, present and future perspectives. Phytochem. Rev. 13, 323–337. https://doi.org/10.1007/s11101-013-9327-z.
Xia, T., Kovochich, M., Brant, J., Hotze, M., Sempf, J., Oberley, T., Sioutas, C., Yeh, J.I., Wiesner, M.R., Nel, A.E., 2006. Comparison of the abilities of ambient and manufactured nanoparticles to induce cellular toxicity according to an oxidative stress paradigm. Nano Lett.. https://doi.org/10.1021/nl061025k.
Yamamoto, Y., Aoyama, S., Hamaguchi, N., Rhi, G.S., 2005. Antioxidative and antihypertensive effects of Welsh onion on rats fed with a high-fat high-sucrose diet. Biosci. Biotechnol. Biochem.. https://doi.org/10.1271/bbb.69.1311.
Yan, J.K., Liu, J.L., Sun, Y.J., Tang, S., Mo, Z.Y., Liu, Y.S., 2015. Green synthesis of

biocompatible carboxylic curdlan-capped gold nanoparticles and its interaction with protein. Carbohydr. Polym.. https://doi.org/10.1016/j.carbpol.2014.10.048.
Yang, Y., Zhang, W., Yang, F., Zhou, B., Zeng, D., Zhang, N., Zhao, G., Hao, S., Zhang, X., 2018. Ru nanoparticles dispersed on magnetic yolk-shell nanoarchitectures with Fe3O4 core and sulfoacid-containing periodic mesoporous organosilica shell as bifunctional catalysts for direct conversion of cellulose to isosorbide. Nanoscale. https://doi.org/10.1039/c7nr07875g.
Yin, M.C., Tsao, S.M., 1999. Inhibitory effect of seven Allium plants upon three Aspergillus species. Int. J. Food Microbiol.. https://doi.org/10.1016/S0168-1605(99)00061-6.
Zhang, L., Jiang, Y., Ding, Y., Povey, M., York, D., 2007. Investigation into the antibacterial behaviour of suspensions of ZnO nanoparticles (ZnO nanofluids). J. Nanoparticle Res.. https://doi.org/10.1007/s11051-006-9150-1.
Zhang, S., Guo, H., Hou, W., Ji, X., Zhang, H., 2018. Synthesis, structure and photocatalytic properties of benzo[ghi] perylenetriimide/graphitic carbon nitride composite. Mater. Lett. 221, 38–41. https://doi.org/10.1016/j.matlet.2018.03.045.
Zhang, Z., Miao, L., Lv, C., Sun, H., Wei, S., Wang, B., Huang, C., Jiao, B., 2013. Wentilactone B induces G2/M phase arrest and apoptosis via the Ras/Raf/MAPK signaling pathway in human hepatoma SMMC-7721 cells. Cell Death Am. Dis. 4 e657.
Zheng, Y., Huang, Y., Shi, H., Fu, L., 2019. Green biosynthesis of ZnO nanoparticles by plectranthus amboinicus leaf extract and their application for electrochemical determination of norfloxacin. Inorg. Nano-Metal Chem. 49, 277–282. https://doi.org/10.1080/24701556.2019.1661441.
Zhivotosky, B., Orrenius, S., 2001. Assessment of apoptosis and necrosis by DNA fragmentation and morphological criteria. Curr. Protoc. cell Biol. Chapter 18, Unit 18.3. https://doi.org/10.1002/0471143030.cb1803s12.